

The biophysical and compositional properties of human basement membranes

Monica S. Schoenenberger¹, Willi Halfter², Alexia Ferrand³, Kathrin Halfter⁴ ,
 Alexandar Tzankov⁵, Hendrik P. N. Scholl^{2,6}, Paul Bernhard Henrich^{2,7} and Christophe A. Monnier² 

1 Swiss Nanoscience Institute, Nano Imaging Lab, University Basel, Switzerland

2 Department of Ophthalmology, University of Basel, Switzerland

3 Imaging Core Facility, Biozentrum of the University of Basel, Switzerland

4 Munich Cancer Registry, Institute of Medical Informatics, Biometry and Epidemiology, Maximilian University Munich, Germany

5 Histopathology and Autopsy, Institute of Medical Genetics and Pathology, University Hospital and University of Basel, Switzerland

6 Institute of Molecular and Clinical Ophthalmology Basel (IOB), Switzerland

7 Università della Svizzera Italiana, Lugano, Switzerland

Keywords

atomic force microscopy; basement membrane; collagen IV; laminin; proteomics

Correspondence

C. A. Monnier, F. Hoffmann-La Roche Ltd.,
 Grenzacherstrasse 124, CH-4070 Basel,
 Switzerland

Tel: +41 797379197

E-mail: christophe.monnier@roche.com

(Received 3 April 2023, revised 14 October
 2023, accepted 16 November 2023)

doi:10.1111/febs.17007

Basement membranes are among the most widespread, non-cellular functional materials in metazoan organisms. Despite this ubiquity, the links between their compositional and biophysical properties are often difficult to establish due to their thin and delicate nature. In this article, we examine these features on a molecular level by combining results from proteomics, elastic, and nanomechanical analyses across a selection of human basement membranes. Comparing results between these different membranes connects certain compositional attributes to distinct nanomechanical signatures and further demonstrates to what extent water defines these properties. In all, these data underline BMs as stiff yet highly elastic connective tissue layers and highlight how the interplay between composition, mechanics and hydration yields such exceptionally adaptable materials.

Introduction

Basement membranes (BMs) represent a widely established class of biological materials that form the backbones of all complex tissues. First described in the literature nearly 50 years ago [1,2], these specialized sheets of extracellular matrix (ECM) are functional materials that fulfill multivalent roles, such as modulating cellular behavior, defining epithelial borders and outlining vasculature, muscle, and nerve fibers [3–7]. Malfunction and fragility therefore lead to severe pathological conditions such as muscular dystrophies or vascular leaks [7–11].

Basement membranes are composite materials whose properties are largely defined by their biochemical constituents, which include collagens (predominantly type

IV), members of the laminin family, proteoglycans, and a variety of other proteins [12–17]. Collagen IV (colIV), an elongated structural protein, exists as a trimer bundle that is segmented into a C-terminal NC1 domain, a triple helical region and a globular N-terminal 7S domain [6,7,18]. These collagen IV fibrils are known to cross-link into a polygonal lattice [5,19,20]. The laminins, on the other hand, polymerize into trimeric rings that form large supramolecular sheets [21]. These two components comprise between 30% and 80% of the total BM proteome [14,15], and are therefore predominantly responsible for BM stability. However, how they contribute to overall material performance is often unclear.

Abbreviations

AFM, atomic force microscopy; BM, basement membrane; CAP-BM, capillary basement membrane; ColIV, collagen type IV; DM, descemet's membrane; ECM, extracellular matrix; ILM, inner limiting membrane; LC, lens capsule; TEM, transmission electron microscopy.

Because of their thin nature, BMs have traditionally been studied by immunohistochemistry or transmission electron microscopy (TEM). While TEM-based measurements have described BMs to be around 100 nm thick [22,23], aggressive tissue processing steps—such as dehydration—are typically needed for these methods. As BMs are highly hydrated materials, it stands to reason that such treatments may alter their appearance and comes to no surprise that methods capable of imaging hydrated BMs yield different results (i.e., thickness values ranging up into the micrometer scale) [24–27]. Namely, this was independently shown on immunostained lens capsules that were imaged by confocal microscopy [28]. More advanced methods such as atomic force microscopy (AFM) and high-resolution fluorescence microscopy have been progressively used as well to investigate specific BMs, notably the inner limiting membrane (ILM, an ocular BM that separates the retina from the vitreous humor). With these approaches, additional features besides structure (i.e., biomechanics) could also be accounted for under immersed and native conditions [24–26], and showed that BMs are bi-layered structures made of a laminin-rich side that promotes epithelial cell adhesion and a colIV-rich side that inhibits epithelial cell adhesion and connects to adjacent stromal layers [29–33]. Further proteomic analyses of these same membranes supplemented these initial observations with compositional attributes and confirmed the presence of traditional BM proteins trimers in the ILM and other BMs (i.e., the Lens Capsule; LC and Descemet's membrane; DM, a BM of the cornea) [14,16,17]. It was further revealed that heterogeneity within the colIV chains (i.e., up to six possible family members) and laminin (i.e., over 20 family members) is extensive and varies as a function of BM type. Likewise, several proteoglycans and up to 20 other ECM components were found as well [14,16,17]. Some BMs even included unexpected components such as a 30% contribution of tubulointerstitial nephritis antigen (TINAG) in vascular [16] and glomerular BMs [34,35], as well as a 50% contribution of TGF β -1-induced glycoprotein (TGFBI) in the DM [17,36]. While stiffness measurements on some of these membranes showed that BMs range in the high kilo- to low mega-Pascal ranges, and around 100 times stiffer than cells [24,37], little is known how these compositional heterogeneities are expressed in the overall biomechanical properties.

In this article, we build upon these studies by comparing the structural, mechanical and compositional varieties between a selection of different BMs. With an initial focus on the ILM, investigations are extended to the DM, the LC, Bruch's membrane (a BM adjacent to the pigment epithelium of the eye) and both capillary (CAP-)

and epidermal BMs. The relationship between composition and biomechanical expression is shown by comparative proteomic, nanomechanical, and elasticity analyses, and by evaluating the role of hydration. Combined, these data show a distinct link between material stiffness, colIV and proteoglycan abundances, and divulge how these parameters are related to water content. Therein, these findings exemplify that BMs are more sophisticated and meticulously tuned than previously described, resulting in an intricately regulated equilibrium between stiffness and elasticity.

Results

BM isolation

Several ocular and non-ocular BMs were isolated from their respective tissues. Initial investigations were focused on the ILM, which exhibits an undulating retinal surface and a smooth vitreous surface (Fig. 1A). Both were maintained after isolation by incubating them in detergent (Fig. 1B) [16,17,27]. These ILMs, as well as the other BMs, appeared under a dissecting microscope as transparent sheets (Fig. 1C) that curl after isolation [16,17,27]. The outer surfaces of the curled ILM as well as the LC and DM represent the retinal, the lens-epithelial and corneal-endothelial surfaces, while the inner surfaces are the vitreous, anterior-chamber and corneal stromal surfaces. We therefore refer to these surfaces as epithelial and stromal surfaces, respectively. Proteomics data confirmed a very low abundance of nuclear, cytosolic, or cytoskeletal proteins in the proteome data lists as exemplified in the Tables S1–S3 (Sheets 1), indicating that the de-cellularization process was effective. Figure 1D shows an ILM mounted on a TEM grid for subsequent elasticity evaluations.

ILM proteomics

Protein composition analyses were conducted on the ILMs from three donors (see Table 1 for details). For proteomics, we relied on a previously established procedure of a simplified LC/MS/MS technique for the LC and DM [16,17]. Of all proteins detected, only ECM proteins were selected as possible BM components, and only proteins that were detected in two of the three ILM samples were considered reliable ILM constituents. The relative abundance of the individual proteins per sample is illustrated in the pie charts in Tables S1–S3, and the mean relative abundance values of all three samples are shown in Fig. 2. These recordings suggest that the collagen trimers make up around

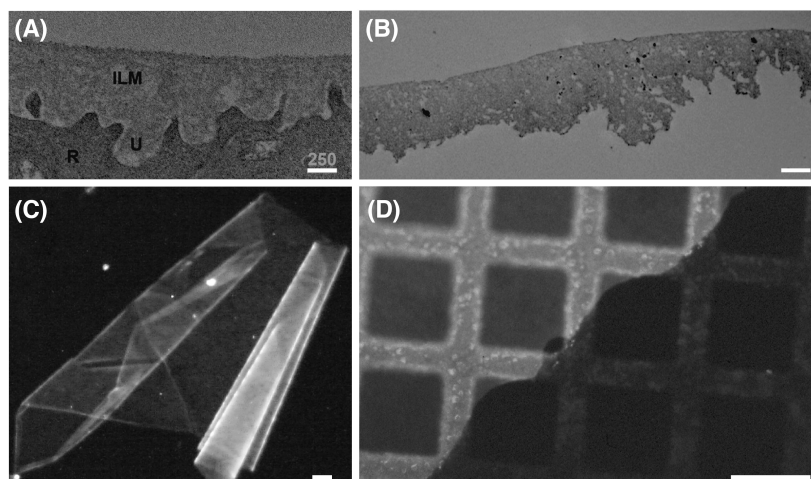


Fig. 1. ILM from adult human eye. The ILM *in situ* is shown in panel (A) (R, retinal cells; U, undulations), and an isolated segment is shown in panel (B). Isolated ILMs, floating freely in PBS, are transparent sheets that curl in a side-specific manner (C). ILMs can be mounted onto TEM grids, on which they cover the open squares without breaking (D). Bars A and B: 250 nm; C: 500 μ m; D: 60 μ m.

Table 1. Samples used for the LC/MS/MS analysis of the ILMs. The table lists age of the donors, their gender, cause of death, the peptide yields after collagenase and trypsin digestion (in μ g), the total number of detected proteins, the number of ECM proteins and the percentage of ECM proteins relative to the total number of proteins. COPD, chronic obstructive pulmonary disease; ICH, intracerebral hemorrhage.

Age, gender	Cause of death	Peptides (μ g)	Proteins (n)	ECM proteins (n)	ECM (%)
38 years m	Anoxic brain injury	52	57	30	53
39 years m	ICH	137	109	48	44
54 years f	COPD	33	82	34	41
Mean		74	83	37	46
SD		45	21	8	5

30% of the total proteome, and the laminin trimers contribute to around 30%. The abundances of laminin and colIV are therefore comparable and together comprise approximately 60% of the total ILM proteome.

This derived proteome is in line with previously published data [14], which were based a more elaborate sample preparation. This included the pre-separation of the BM proteins by SDS/PAGE and the extraction of proteins from 17 cut-out gel segments for each sample, which each required an individual LC-MS/MS run. For our analyses, this would have meant a total of 51 LC-MS/MS runs as compared to only 3 runs using the current procedure. When comparing the data from both sample preparations side-by-side, the relative abundance of laminin and colIV family members are about equal for the ILM, with both proteins representing the most

prominent components. Further, the laminin and colIV chain compositions are identical in both analyses. A major difference was the number of protein hits: in difference to the present analysis with up to 40 ECM protein IDs, the previous analysis resulted in over 200 IDs, whereby the majority of the hits were proteins in minute quantities [14]. 16% of all proteins in the previous analysis were ECM proteins as compared to 46% in the current analysis.

Elasticity, ionic strength and hydration

In a first step, we probed the ILMs' elasticity and expandability by indenting freely suspended membranes with an AFM tip (Fig. 3). Membrane sidedness was visualized by immunostaining for colIV and laminin (Fig. 3A) before mounting them on TEM grids with a single hole aperture of 50 μ m (Fig. 3B). This assured that they were suspended over an open space for indentation with a constant force of 1 μ N (Fig. 3C). A film of nitrocellulose (Parlodion, NC) with a thickness of 100 nm was used as a reference material.

When air-dried, the ILM exhibited a very steep stress-strain slope (Fig. 3D), indicating an ultralow elasticity, while the nitrocellulose film slope was slightly less steep. Conversely, the stress-strain curves were substantially shallower on an ILM immersed in PBS, while the nitrocellulose film remained unchanged (Fig. 3E). Moreover, this ILM could be pressed down without rupture for more than 3 μ m. While the effective point of rupture was never reached (i.e., due to the limited range of the AFM piezo), the ILM still expanded by at least 33% without visible damage and returned to its original conformation once the load was withdrawn. This process could be repeated over

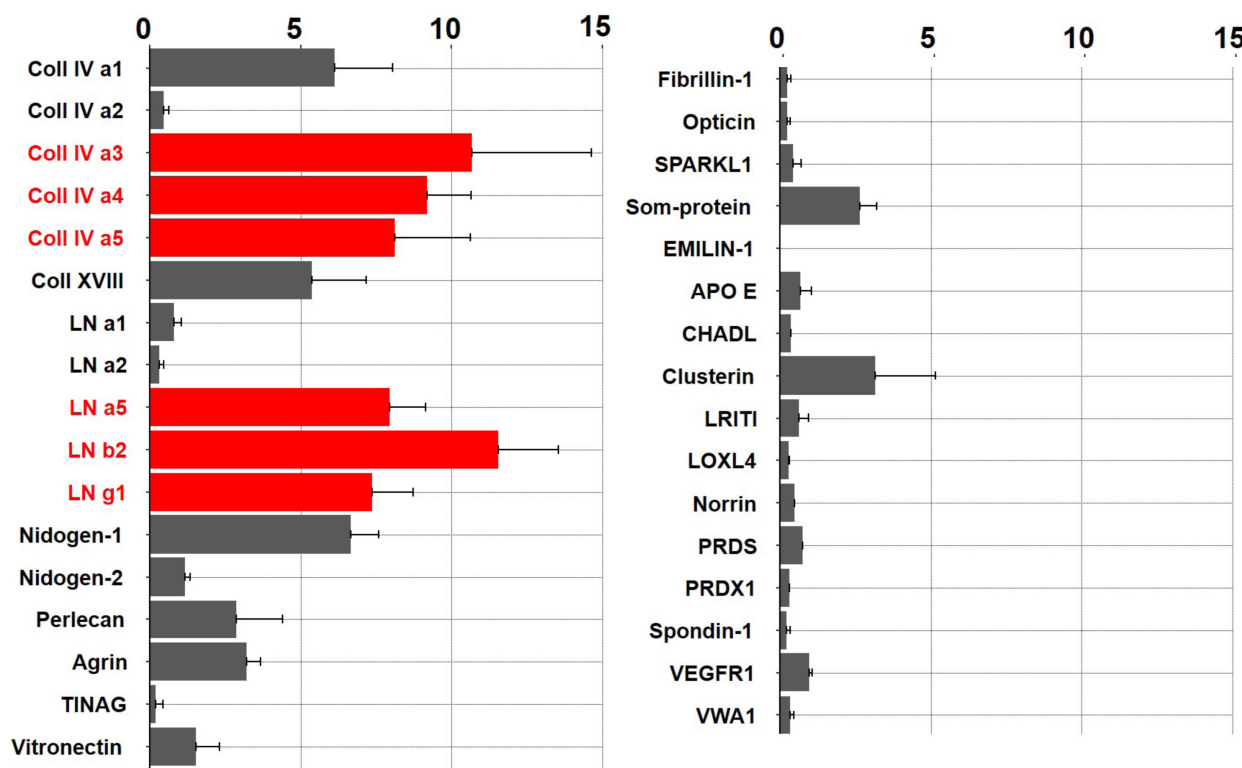


Fig. 2. The proteome of the adult human ILM. The concentrations of individual protein components are shown in percent to the total ILM proteome. CHADL, chondroadherin-like protein; Coll, collagen; LN, laminin; LOXL4, lysyl oxidase-homolog 4; LRTI, leucine-rich repeat and immunoglobulin-like domain and trans-membrane-containing protein 1; PRDX, peroxiredoxin; Som-protein, somatomedin and trombospondin type 1-domain containing protein; TINAG, tubulointerstitial nephritis antigen; VEGFR1, VEGF receptor 1; VWA1, von Willebrand Factor A-containing protein. The error bars represent the standard deviation of the mean value ($n = 3$).

20 times without rupturing the material, highlighting its elastic nature and to what degree water influences it.

In a second step, we conducted side-specific nanoindentation experiments to narrow down these considerations (Fig. 4). Initial trials in PBS revealed a stiffness distribution pattern similar to previously reported results (i.e., the epithelial side of the membrane being approximately twice as stiff as the stromal side, Fig. 4A) [29–31]. We then incubated the same membrane in glutaraldehyde to evaluate the remaining level of non-cross-linked material, i.e., by measuring to what degree the material stiffness changed (Fig. 4B). Surprisingly, stiffness values remained unchanged, suggesting that all BM components are already cross-linked to a maximum degree or—arguably—that additional cross-linking does not significantly contribute to overall material stiffness. However, varying the ionic strength of the solvent—a basic measure to study water content and distribution—yielded intriguing results (Fig. 4C): membrane stiffness substantially increased when the membrane was immersed in

hypertonic solutions, whereas hypotonic concentrations led to a minor degree of softening. The most captivating point of the trials however was that this effect only occurred on the epithelial side of the membrane, whereas the stromal side remained unaffected. This is indicative that other BM-specific, water-binding components (i.e., proteoglycans) are predominantly located on the epithelial side of the membrane.

We therefore explored the overall impact of water on BM structure in more detail (Fig. 4D). Other BMs (i.e., the LC and the DM) were included into these examinations, and their respective thicknesses were determined by sensing the top of the BMs and the underlying glass surface with the AFM tip. The LC was by far the thickest BM, followed by the DM and the ILM. All BMs were then dehydrated either in an increasing series of dilutions of alcohol (i.e., as it would be used in standard TEM sample preparation protocols) or by air-drying. Independent of the dehydration process, all membranes shrank by 68–85%. Intriguingly, this process was reversible, with a rehydration of the very same samples leading to a complete

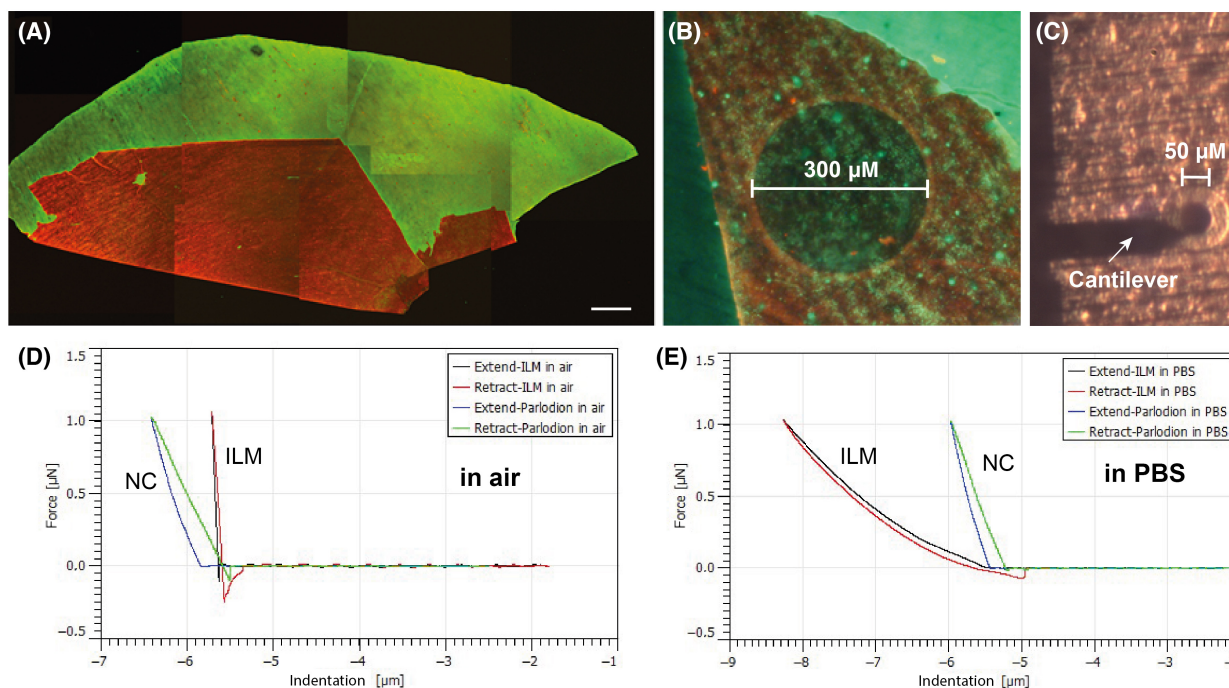


Fig. 3. Sidedness and elastic micro-indentation measurements of the ILM. Prior to analysis, the ILM (A) was immunostained with antibodies to laminin (red) and colIV $\alpha 3,4,5$ (green). Both the retinal (red) and the vitreal sides (green) were exposed. This ILM was mounted over a single-hole TEM grid (diameter = 300 μm , B), again showing the retinal (red) and the vitreal sides (green). An AFM cantilever, which is clearly visible next to the 50 μm hole of the support grid (C), was used to indent the suspended membrane. Stiffness measurements on an air-dried ILM and a nitrocellulose film (NC) show very steep stress/strain curves (D). When immersed in PBS, the nitrocellulose curve remains consistent, while the hydrated ILM becomes hyper-extendable (i.e., by over 3 μm), with an increase of its surface area by 33% without rupturing (E). Bars A: 500 μm .

recovery of their original thicknesses within minutes. These values are also relatable to those derived from fluorescence super-resolution microscopy images of a fully hydrated ILM (Fig. 4E).

Combining compositional with mechanical attributes

To follow up on these observations, further nanomechanical measurements were conducted on these and other BMs, such as CAP- and epidermal BMs: Stiffness values from materials originating from the same donors were measured in one round to maximize comparative meaningfulness (Fig. 5), and both BM sides were examined whenever possible. Results showed that for the epithelial sides the DM (mean = 670.4 ± 91.4 kPa, $n = 3$, 758 force curves) was the stiffest of all investigated BMs, followed by the ILM (mean = 445.0 ± 26.4 kPa, $n = 3$, 760 force curves). The LC (mean = 187.6 ± 37.2 kPa; $n = 3$, 573 force curves; only segments of the frontal part of the lens were probed) expressed a lower stiffness profile, whereas Bruch's membrane (mean = 88.7 ± 17.7 kPa, $n = 2$, 363 force curves) and the epidermal BMs

(mean = 49.2 ± 17.3 kPa, $n = 2$, 287 force curves) were the softest. For the stromal sides of the tested BMs, the ILM was the stiffest (mean = 195.9 ± 46.4 kPa; $n = 3$, 515 force curves), followed by the DM (mean = 160.8 ± 65.9 kPa, $n = 3$, 807 force curves), the LC (mean = 80.3 ± 3.6 kPa, $n = 3$, 8329 force curves), the Bruch's membrane (mean = 57.7 ± 15.2 kPa, $n = 2$, 326 force curves) and the vascular BM (mean = 46.9 ± 36.8 kPa, $n = 3$, 543 force curves). For comparison, we also assayed fiber cartilage from human meniscus (mean = 149.0 kPa, $n = 1$, 119 force curves), which was slightly softer than the LC. All investigated BMs expressed the same side-specific stiffness distribution as previously observed on multiple occasions.

To identify possible root causes of these variations, we conducted comparative proteomic analyses on these same BMs and correlated stiffness data to compositional attributes. For this, a unified analysis technique was applied to reveal what proteins are shared or altered between the materials (Fig. 6) [16,17]. The resulting data showed that high stiffness, as seen in the DM and ILM, rather correlates inversely with high colIV concentrations. Namely, the BM with the

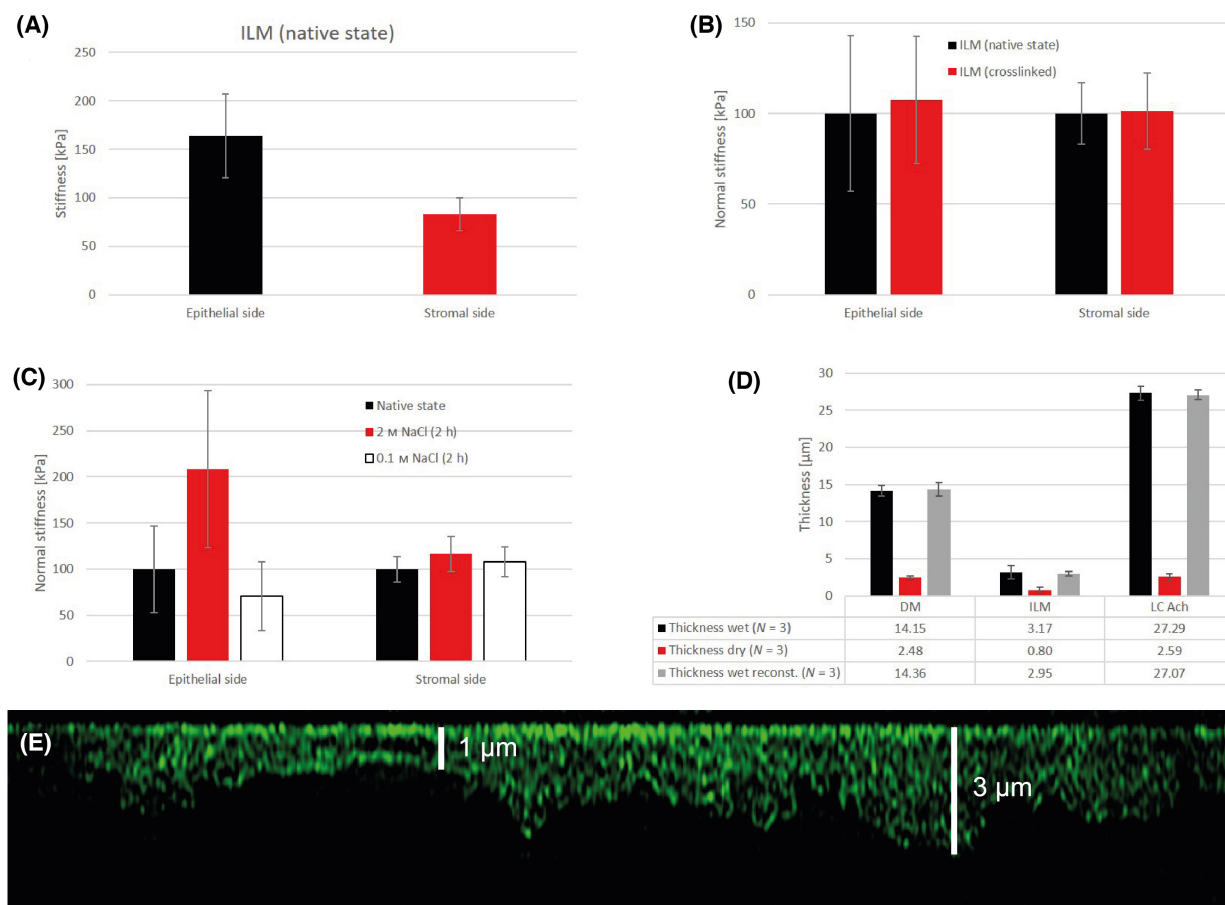


Fig. 4. Cross-linking and hydration. When probing both ILM surfaces of the same membrane ($n = 1$, 576 force curves per surface), the stromal side is softer (A, red columns) than the epithelial sides (A, black columns). Treatment does not affect these properties (B). Major increases in stiffness are seen when the membrane is incubated in hypertonic solvents, while hypotonic ones lead to stiffness reduction (C, a modulation that is only observed on the epithelial side of the membrane). Measurements on original, dehydrated and fully hydrated DMs ($n = 3$), ILMs ($n = 3$) and LCs ($n = 3$) show how massively overall thickness changes once water is removed, and how the original state is regained when added (D). A fully hydrated ILM is seen by fluorescence super-resolution microscopy in (E). Note that the undulating and smooth outlines of the respective stromal and epithelial surfaces were identical to those seen by TEM (i.e., to be compared with Fig. 1A,B). Each column represents the average calculated for each BM, and the error bars represent the standard deviation of the mean value.

highest colIV concentration (i.e., the LC with 70%) was softest, while the BM with the lowest concentration (i.e., the DM with 11%) was stiffest. Nonetheless, it should be noted that the trimer composition may play a role in the overall stiffness profile, as collagen IV $\alpha 3,4,5$ was by far the dominant colIV trimer in the DM and ILM. In this context, previous reports have shown that colIV $\alpha 3,4,5$ is mechanically more robust than the classical $\alpha 1,1,2$ trimer [18], the composition typically found in the other BMs. A further correlation between stiffness and protein composition was apparent in the proteoglycan content [16,17], where a decreasing stiffness profile correlated with an increasing perlecan concentration. This is in agreement with previous studies, where de-glycosylation of heparan

sulfate proteoglycans resulted in significantly reduced BM thickness and increased stiffness [24,26]. These measurements explain our observations with regards to ionic strength and hydration, and underline water as an essential structural component and main driver of membrane mechanics.

Discussion

The biophysical properties of the ILM, and BMs in general, are defined by many factors. In this article, we piece together how some of them – notably nanomechanical and proteomic properties – affect these properties, and show how specific BM factors play a more distinct role than might first meet the eye.

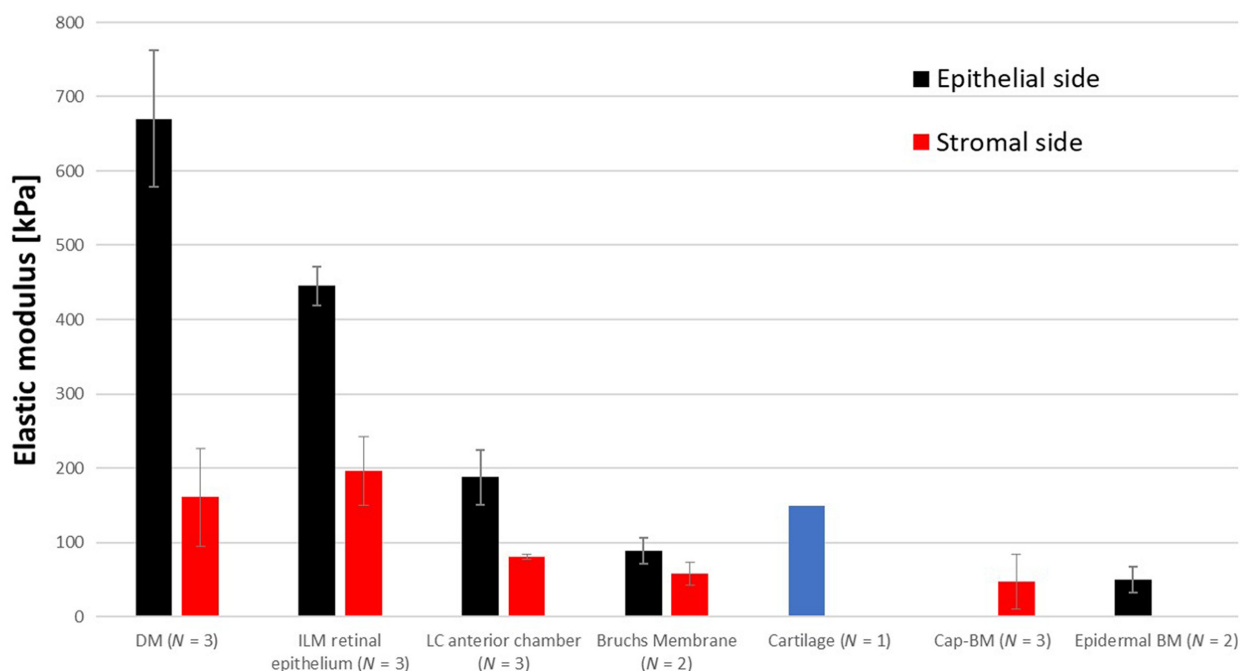


Fig. 5. The nanomechanical profiles of human BMs. The highest stiffness values (in kPa) are found in the DM ($n = 3$), followed by the ILM ($n = 3$), the LC towards the anterior chamber (LC Ach, $n = 3$), Bruch's Membrane ($n = 3$) and finally the capillary (CAP-BM, $n = 3$) and epidermal BMs ($n = 2$). The stromal side of the membrane (red columns) is recurrently softer than the epithelial side (black columns) in all examined membranes where side-specific measurements were feasible. For capillary BMs, only the stromal side of intact capillaries was accessible. For epidermal BMs, the stromal sides remained inseparably attached to a layer of dermis, therefore only allowing the probing of the epithelial side of these BMs. Cartilage from human meniscus ($n = 1$) is included as a comparative tissue (blue). Each column represents the average elastic modulus calculated for each BM, and the error bars represent the standard deviation of the mean value.

Mechanical measurements show that the DM is by far the stiffest BM of all tested samples. As its main function involves supporting the cornea by protecting the eyeball from trauma, it is plausible that it should be exceptionally stiff. Second in line on the stiffness scale was the ILM, followed by the LC, while Bruch's membrane—which separates the highly vascularized choroid from the retinal pigment epithelium—and both the epidermal and CAP-BMs were last in line. In contrast to the DM, elasticity is essential to these membranes, as they need to retract and expand frequently and repeatedly. On the other hand, insufficient Bruch's membrane stiffness predisposing to breaches in membrane integrity may play a role in the development of exudative age-related macular degeneration.

These same measurements show an inversely proportional to the respective colIV concentrations, and that glutaraldehyde treatment does not induce any apparent mechanical effects. This further questions whether such membranes are already fully crosslinked or that BM stiffness is significantly related to covalent crosslinking in general. Conversely, water content correlates to an exceedingly high degree with both membrane mechanics and elasticity. This is apparent in the mechanical

stiffening induced by hypertonic solutions and reversal under opposite conditions. These assumptions are further underlined by the measured changes in BM thickness once water is actively removed. As only the epithelial side of the membrane is susceptible to changes in tonicity, we surmise that the charged components of the BM, namely its water-binding proteoglycans, are predominantly located there. This remains plausible when pondering their role as liaisons between laminin and colIV. In return, lower BM stiffness trends directly correlate with elevated proteoglycan concentrations, consequently attesting that water is a key player and contributor to BM structure and elasticity.

Taken together, these results highlight BMs as layered, elastic and adaptable materials, and offer an incremental step in deeper understanding how the properties they require to fulfill their roles come to be.

Materials and methods

BM sources and preparation

Human donor eyes and skin samples were obtained from CORE, the Center of Organ Recovery and Education in

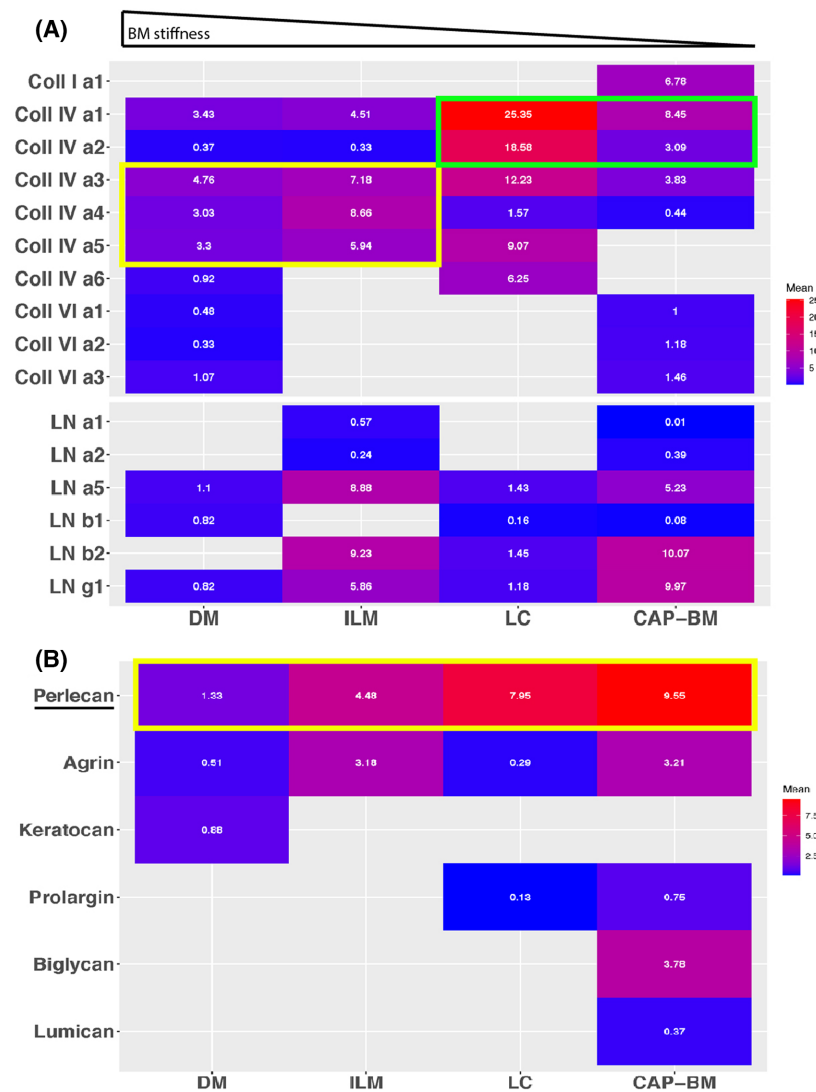


Fig. 6. Compositional comparisons between the basement membrane proteomes. The compositional percentages of the collagen IV and laminin family members are listed along with those of proteoglycans. The stiffest BM is on the left (i.e., the DM), and the softest one on the right (i.e., the CAP-BM). The LC, with the highest overall concentration of collagen IV (over 70% of the entire ECM proteome), is not the stiffest BM in this selection, whereas the stiffest BMs (i.e., the DM and ILM) contain exclusively collagen IV a3,4,5. A closer look at the proteoglycans shows that higher concentrations of perlecan correlate with a decreasing BM stiffness.

Pittsburgh, USA, and from the Institute of Medical Genetics and Pathology of the University Hospital and University of Basel, Switzerland. The use of human eyes for this project was approved by the Internal Review Board of the University of Pittsburgh (IRB protocol #0312072) and by the Ethics Commission of Northern and Central Switzerland (IRB protocol #279/11). Written consent for tissue usage for research was given by the participants during their lifetime or by their next of kin.

The time intervals between death and organ harvesting ranged between 2 and 7 h, with their delivery to the laboratory taking place the following day after testing for HIV and hepatitis. LCs, DMs from corneas, ILMs and CAP-BMs were isolated from donor eyes as described previously [14,16,17,24]. Bruch's membranes were isolated from the retinal pigment epithelium by incubation in Triton X-100 followed by 0.5% deoxycholate overnight. The epidermal surfaces of skin BMs were exposed by incubating skin samples in 1 M salt or 0.5 M

EDTA and peeling off the epidermis, resulting in the BMs resting on the underlying dermis [38]. Upon isolation, the BMs were stable and stored in PBS supplied with 0.01% sodium azide at 4 °C until analyzed. Cartilage samples from meniscus were de-cellularized by incubating them in 2% Triton X-100 and deoxycholate overnight. We only analyzed samples from donors of similar age given age-dependent variations in protein compositions [14]. The cartilage and one of the skin samples were obtained during a meniscus surgery and a mole removal by a dermatologist.

Proteomics

Isolated ILMs were spun down at 1000 g (RCF) for 3 min and washed three times. The pellet was collected in 150 µL of PBS. Fifty microliter of collagenase (1000 U·mL⁻¹; type VII; Sigma-Aldrich, St. Louis, MO, USA) were added, and the sample incubated for 24 h at 37 °C. Next, the proteins were

reduced with 10 mM DTT at 37 °C for 1 h and alkylated with 50 mM iodoacetamide for 15 min at room temperature. Protein digestion was performed by incubation of the sample with 1 µL trypsin (sequencing grade; Promega, Madison, WI, USA) at 37 °C overnight. This digestion regime resulted in complete BM solubilization. The digest was then desalted on a C18 microspin column (The Nest Group, Southborough, MA, USA) according to the manufacturer's recommendations. Peptide absorbance was measured at 280 nm and peptide concentration was calculated according to Wisniewski *et al.* [39]. Six micrograms were sufficient for the three technical LC-MS/MS replicate runs. LC-MS/MS analysis was performed on either an Orbitrap Elite or Orbitrap Classic (Thermo Scientific, Reinach, Switzerland) interfaced with an EASY-nLC 1000 pump connected to a C18 column (75 µm × 15 cm) packed with 2.4 µm Reprosil beads [39]. For each analysis, equal peptide material (2 µg) was injected in triplicates onto the capillary column. Chromatography and mass spectrometric parameters corresponded to the previously described methods [40].

The LC/MS/MS data were searched against the SWISS-PROT protein sequence database (www.uniprot.org, as of September 2023). The Mascot and Sequest HT search engines were run via PROTEOME DISCOVERER 1.4 (Thermo Scientific). Search parameters were set to carbamidomethylated cysteines as fixed modification, whereas oxidized methionines and protein N-terminal acetylation were set to as variable modifications. For peptide identifications, a false discovery rate of 1% was set. Label-free protein quantification was done by integrating for each identified peptide the ion intensity under the elution curve, and the total intensity for a given protein was calculated using PROTEOME DISCOVERER 1.4 [41]. Each data set was analyzed in three technical replicates. Biological sample replicates comprised three pairs of eyes.

The evaluation of the proteome data for the ILM followed a previously established procedure that was used for the analysis of the LC, the DM and vascular BMs [16,17]. Of all proteins detected, only ECM proteins were selected as possible BM components, and only proteins that were detected in two of the three ILM samples were considered reliable ILM constituents.

For relative protein quantification, the ion intensity for the identified peptides was integrated as area under the curve from which the total intensity for a given protein was calculated using PROTEOME DISCOVERER 1.4, a standard procedure for label-free protein quantification in mass spectrometry [41]. The abundance of a given BM protein in each sample was expressed as percentage relative to the total ECM protein of each sample that was set to 100%.

Immunohistochemistry

ILM segments were spread onto 1.5 mm thick glass cover slips (Fisher Scientific, Waltham, MA, USA) coated with

5 µg·mL⁻¹ poly-lysine (Sigma-Aldrich). For firm attachment of the BM sheets, the cover slips—resting on glass slides—were centrifuged at 112 *g* (RCF) for 5 min. The whole mounts were washed twice with 1% BSA, 0.01% Triton-X-100 and stained with two polyclonal antisera to collagen IV (Rockland, Gilbertsville, PA, USA and ICN/Cappel, Aurora, CO, USA), laminin (Sigma-Aldrich), and a mouse monoclonal antibody to the 7S domain of collagen IV a3 (Mab J3-2; kindly provided by N. Sundarraj) [42]. The specified antibody is also available from Sigma-Aldrich (SAB4200500). Y. Sado provided rat monoclonal antibodies raised against chain-specific NC1 peptides of collIV [43]. The secondary antibodies were Cy3, AMCA- or Alexa-Fluor 488-labeled goat anti-rabbit, goat anti-mouse, or mu-chain-specific goat anti-mouse antibodies (Jackson ImmunoResearch, West Grove, PA, USA; and Life Technologies, Carlsbad, CA, USA). For each antibody step, the suspended BMs were incubated overnight. Micrographs were recorded with an Olympus FluoView 1000 confocal microscope (Olympus Corporation, Tokyo, Japan).

Three-dimensional structured illumination microscopy (3D-SIM) was performed on a DeltaVision OMX-Blaze V4 system (Cytiva, Marlborough, MA, USA). Images were acquired using a Plan Apo N 60×, 1.42 NA oil immersion objective lens (Olympus Corporation) and 4 liquid-cooled sCMOS cameras (pco.edge 5.5, full frame 2560 × 2160; PCO). Exciting light was directed through a movable optical grating to generate a fine-striped interference pattern on the sample plane. The pattern was shifted laterally through five phases and three angular rotations of 60° for each Z section. The laser lines were used during acquisition and the optical Z sections were separated by 0.125 µm. Laser power was attenuated to 10% and exposure times were typically between 3 and 100 ms, and the power of each laser was adjusted to achieve optimal intensities of between 5000 and 8000 counts in a raw image of 15-bit dynamic range at the lowest laser power possible to minimize photobleaching. Multichannel imaging was achieved through sequential acquisition of wavelengths by separate cameras.

Atomic force microscopy

DMs, LCs, ILMs, Bruch's membranes, epidermal and CAP-BMs were spread onto poly-lysine-coated Superfrost-plus glass slides (Fisher Scientific) as described [14,16,17] and firmly attached onto the substrates by centrifugation. ILM samples were also mounted onto one-hole gold TEM grids (Gilder grids, GA50-G3 with a 50 µm aperture, Micro to Nano, Haarlem, the Netherlands). For the elasticity measurements of the freely suspended ILMs, the edges of the grids were glued onto splinters of 1 mm glass cover slip, and the ILM preparations were kept incubated in PBS. Measurements were performed using a JPK NanoWizard 4 AFM (Bruker Nano GmbH, Berlin, Germany). Sharp silicon tips with radii of around 10 nm mounted on

standard monolithic silicon beam-shaped cantilevers with nominal spring constants of $3 \text{ N}\cdot\text{m}^{-1}$ were used, and their spring constants were determined in PBS prior to every experiment by using the Sader method [44]. Force spectroscopy was generally performed with a load of 2 nN, with indentation depths ranging between 50 and 400 nm, and thus in accordance with Buckle's one-tenth law (i.e., indentation depth < 10% of total material thickness) to mitigate any influence of underlying layers [45]. The loading and unloading speed was set to $2 \mu\text{m}\cdot\text{s}^{-1}$. Three samples of each BM were probed, and force-displacement curves were recorded at three different locations on both epithelial and stromal sides (whenever possible) with a scanning area of $10 \times 10 \mu\text{m}$. From these data, the elastic moduli were calculated with the JPK DATA PROCESSING software (Bruker Nano GmbH) by using the Hertz model.

Skin samples tested by AFM were from a non-mole area of the skin and exposed to high-salt or EDTA concentrations prior to AFM testing [38]. They were tested for their stiffness on the exposed epidermal sides.

Acknowledgements

We would like to thank Ralph Schoch from the Institute of Medical Genetics and Pathology at the University Hospital of Basel for his excellent technical support in collecting donor eyes, as well as Dr Nir-mala Sudarraj from the University of Pittsburgh for the J1 mAb to collagen IV $\alpha 3$. We would also like to acknowledge the help of Paul Jenö and the Proteomics Core Facility of the Biozentrum, University of Basel.

The project was made possible by the generous support of Bayer (Switzerland) Ltd through an "Investigator-Initiated, Independent Research Grant".

HPNS is supported by the Swiss National Science Foundation (Project funding: "Developing novel outcomes for clinical trials in Stargardt disease using structure/function relationship and deep learning" #310030_201165, and National Center of Competence in Research Molecular Systems Engineering: "NCCR MSE: Molecular Systems Engineering (phase II)" #51NF40-182895), the Wellcome Trust (PINNACLE study), and the Foundation Fighting Blindness Clinical Research Institute (ProgStar study).

Conflict of interest

HPNS is a member of the Scientific Advisory Board of: Boehringer Ingelheim Pharma GmbH & Co; Claris Biotherapeutics Inc.; Eluminex Biosciences; Gyroscope Therapeutics Ltd.; Janssen Research & Development, LLC (Johnson & Johnson); Novartis Pharma AG (CORE); Okuvision GmbH; ReVision Therapeutics Inc.; and Saliogen Therapeutics Inc., and a consultant

of: Alnylam Pharmaceuticals Inc.; Gerson Lehrman Group Inc.; Guidepoint Global, LLC; and Intergalactic Therapeutics Inc. HPNS is a member of the Data Monitoring and Safety Board/Committee of Belite Bio (CT2019-CTN-04690-1), F. Hoffmann-La Roche Ltd (VELODROME trial, NCT04657289; DIAGRID trial, NCT05126966; HUTONG trial) and member of the Steering Committee of Novo Nordisk (FOCUS trial; NCT03811561). HPNS is the co-director of the Institute of Molecular and Clinical Ophthalmology Basel (IOB), which is constituted as a non-profit foundation and receives funding from the University of Basel, the Universitätsspital Basel (USB), Novartis, and the government of Basel-Stadt.

All arrangements have been reviewed and approved by the University of Basel (Universitätsspital Basel, USB) and the Board of Directors of the Institute of Molecular and Clinical Ophthalmology Basel (IOB) in accordance with their conflict of interest policies. Compensation is being negotiated and administered as grants by the University Hospital Basel, which receives them on its proper accounts.

CAM is currently employed by F. Hoffmann-La Roche Ltd. This affiliation however was realized after this Study was concluded at the Universitätsspital Basel.

Author contributions

WH, CAM, and MSS conceived and designed the experiments. MSS, AF, CAM, and KH carried out the experiments. MSS, WH, KH and CAM analyzed the data. AT, HPNS, WH, and PBH secured access to human material and contributed to sample preparation. PBH helped supervise the project. MSS, WH and CAM wrote the manuscript with input from all authors.

Data availability statement

The data that support the findings of this study are available from the authors upon reasonable request.

References

- 1 Kefalides NA (1971) Chemical properties of basement membranes. *Int Rev Exp Pathol* **10**, 1–39.
- 2 Vrancko R (1974) Basal lamina scaffold-anatomy and significance for maintenance and orderly tissue structure. *Am J Pathol* **77**, 314–346.
- 3 Yurchenco PD (2011) Basement membranes; cell scaffolds and signaling platforms. *Cold Spring Harb Perspect Biol* **3**, a004911.

- 4 Halfter W & Yip J (2014) An organizing function of basement membranes in the developing nervous system. *Mech Dev* **133**, 1–10.
- 5 Mak KM & Mei R (2017) Basement membrane type IV collagen and laminin: an overview of their biology and value as fibrosis biomarkers of liver disease. *Anat Rec* **300**, 1371–1390.
- 6 Kalluri R (2003) Basement membranes: structure, assembly and role in tumour angiogenesis. *Nat Rev Cancer* **3**, 422–433.
- 7 LeBleu VS, MacDonald B & Kalluri R (2007) Structure and function of basement membranes. *Exp Biol Med* **232**, 1121–1129.
- 8 Miner JH & Yurchenco PD (2004) Laminin functions in tissue morphogenesis. *Annu Rev Cell Dev Biol* **20**, 255–284.
- 9 Miner JH, Cunningham J & Sanes JR (1998) Roles of laminin in embryogenesis: exencephaly, syndactyly, and placentopathy in mice lacking the laminin alpha5 chain. *J Cell Biol* **143**, 1713–1723.
- 10 Mao M, Alavi MV, Labelle-Dumais C & Gould DB (2015) Type IV collagens and basement membrane diseases: cell biology and pathogenic mechanisms. *Curr Top Membr* **76**, 61–116.
- 11 Seikaguchi K & Yamada KM (2018) Basement membranes in development and disease. *Curr Top Dev Biol* **130**, 143–191.
- 12 Timpl R & Brown JC (1996) Supramolecular assembly of basement membranes. *Bioessays* **18**, 123–132.
- 13 Erickson AC & Couchman JR (2000) Still more complexity in mammalian basement membranes. *J Histochem Cytochem* **48**, 1291–1306.
- 14 Uechi G, Sun Z, Schreiber EM, Halfter W & Balasubramani M (2014) Proteomic view of basement membranes from human retinal blood vessels, inner limiting membranes, and lens capsules. *J Proteome Res* **13**, 3693–3705.
- 15 Randless MJ, Humphries MJ & Lennon R (2017) Proteomic definitions of basement membrane composition in health and disease. *Matrix Biol* **57**, 12–28.
- 16 Halfter W, Moes S, Asgeirsson DO, Oertle P, Melo-Herraiz E, Plodinec M, Jenoe P & Henrich PB (2018) Diabetes-related changes in the protein composition and biomechanical properties of human retinal vascular basement membranes. *PLoS One* **12**, e0189857.
- 17 Halfter W, Moes S, Halfter K, Schoenenberger MS, Monnier CA, Kalita J, Asgeirsson D, Binggeli T, Jenoe P, Scholl HPN *et al.* (2020) The human Descemet's membrane and lens capsule: protein composition and biomechanical properties. *Exp Eye Res* **201**, 108326.
- 18 Khoshnoodi J, Pedchenko V & Hudson BG (2008) Mammalian collagen IV. *Microsc Res Tech* **71**, 357–370.
- 19 Timpl R, Wiedeman H, van Delden V, Furthmayr H & Kuehn K (1981) A network model for the organization of type IV collagen molecules in basement membranes. *Eur J Biochem* **120**, 203–211.
- 20 Wu Y & Ge G (2019) Complexity of type IV collagens: from network assembly to function. *Biol Chem* **400**, 565–574.
- 21 Beck K, Hunter I & Engel J (1990) Structure and function of laminin: anatomy of a multidomain glycoprotein. *FASEB J* **4**, 148–160.
- 22 Yurchenco PD & Ruben GC (1987) Basement membrane structure in situ: evidence for lateral associations in the type IV collagen network. *J Cell Biol* **105**, 2559–2568.
- 23 Ruben GC & Yurchenco PD (1994) High resolution platinum-carbon replication of freeze-dried basement membrane. *Microsc Res Tech* **28**, 13–28.
- 24 Candiello J, Balasubramani M, Schreiber EM, Cole GJ, Meyer U, Halfter W & Lin H (2007) Biomechanical properties of native basement membranes. *FEBS J* **274**, 2897–2908.
- 25 Balasubramani M, Schreiber EM, Candiello J, Balasubramani GK, Kurtz J & Halfter W (2010) Molecular interactions in the retinal basement membrane system: a proteomic approach. *Matrix Biol* **29**, 471–483.
- 26 Candiello J, Cole GJ & Halfter W (2010) Age-dependent changes in the structure, composition and biophysical properties of a human basement membrane. *Matrix Biol* **29**, 402–410.
- 27 To M, Goz A, Camenzind L, Oertle P, Candiello J, Sullivan M, Henrich PB, Loparic M, Safi J, Eller A *et al.* (2013) Diabetes-induced morphological, biomechanical, and compositional changes in ocular basement membranes. *Exp Eye Res* **116**, 298–307.
- 28 Danysh BP & Duncan MK (2008) The lens capsule. *Exp Eye Res* **88**, 151–166.
- 29 Henrich PB, Monnier CA, Halfter W, Haritoglou C, Strauss RW, Lim RY & Loparic M (2012) Nanoscale topographic and biomechanical studies of the human internal limiting membrane. *Invest Ophthalmol Vis Sci* **53**, 2561–2570.
- 30 Henrich PB, Monnier CA, Loparic M & Cattin PC (2013) Material properties of the internal limiting membrane and their significance in chromovitrectomy. *Ophthalmologica* **230** (Suppl. 2), 11–20.
- 31 Halfter W, Monnier C, Müller D, Oertle P, Uechi G, Balasubramani M, Safi F, Lim R, Loparic M & Henrich PB (2013) The bi-functional organization of human basement membranes. *PLoS One* **8**, e67660.
- 32 Halfter W, Oertle P, Monnier CA, Camenzind L, Reyes-Lua M, Hu H, Candiello J, Labilloy A, Balasubramani M, Henrich PB *et al.* (2015) New concepts in basement membrane biology. *FEBS J* **282**, 4466–4479.
- 33 Halfter W, Zhang P, Schreiber E & Balasubramani M (2013) Protein composition and biomechanical

- properties of in vivo-derived basement membranes. *Cell Adh Migr* **7**, 64–71.
- 34 Butkowsky RJ, Langeveld JP, Wieslander J, Brentjens JR & Andres GA (1990) Characterization of a tubular basement membrane component reactive with autoantibodies associated with tubulointerstitial nephritis. *J Biol Chem* **266**, 21091–21098.
- 35 Kalfa TA, Thull JD, Butkowsky RJ & Charonis AS (1994) Tubulointerstitial nephritis antigen interacts with laminin and type IV collagen and promotes cell adhesion. *J Biol Chem* **269**, 1654–1659.
- 36 Skonier J, Neubauer M, Madisen L, Bennet K, Plowman GD & Purchio AF (1992) cDNA cloning and sequence analysis of beta Ig-H3, a novel gene induced in an adenocarcinoma cell line after treatment with transforming growth factor beta. *DNA Cell Biol* **11**, 511–522.
- 37 Janmey PA & McCulloch CA (2007) Cell mechanics: integrating cell response to mechanical stimuli. *Annu Rev Biomed Eng* **9**, 1–34.
- 38 Behrens DT, Villone D, Koch M, Brunner G & Sorokin L (2012) The epidermal basement membrane is a composite of separate laminin or collagen IV-containing networks connected by aggregated perlecan, but not by nidogens. *J Biol Chem* **287**, 18700–18709.
- 39 Wisniewski JR, Zougman A, Nagaraj N & Mann A (2009) Universal sample preparation method for proteome analysis. *Nat Methods* **6**, 359–362.
- 40 Robitaille AM, Christen S, Shimobayashi M, Cornu M, Fava LL, Moes S, Prescianotto-Baschong C, Sauer U, Jenoe P & Hall MN (2013) Quantitative phosphoproteomics reveal mTORC1 activates de novo pyrimidine synthesis. *Science* **339**, 1320–1323.
- 41 Neilson KA, Ali NA, Muralidharan S, Mirzaei M, Mariani M, Assadourian G, Sluyter SC & Haynes PA (2011) Less label, more free: approaches in label-free quantitative mass spectrometry. *Proteomics* **11**, 535–553.
- 42 Sundarraj N & Wilson J (1982) Monoclonal antibody to human basement membrane collagen type IV. *Immunology* **47**, 133–140.
- 43 Sado Y, Kagawa M, Kishiro Y, Sugihara K, Naito I, Seyer JM, Sugimoto M, Oohashi T & Ninomiya Y (1995) Establishment by the rat lymph node method of epitope-defined monoclonal antibodies recognizing the six different α chains of human type IV collagen. *Histochem Cell Biol* **104**, 267–275.
- 44 Sader JE, Chon JW & Mulvaney P (1999) Calibration of rectangular atomic force microscope cantilevers. *Rev Sci Instrum* **70**, 3967–3969.
- 45 Westbrook JH (1973) *The Science of Hardness Testing and its Research Applications*. American Society for Metals, Metals Park, OH.

Supporting information

Additional supporting information may be found online in the Supporting Information section at the end of the article.

Table S1. LC/MS/MS protein composition data from a 38-year-old male ILM. Sheet 1 summarizes the total proteome, and selected ECM proteins are listed in Sheet 2.

Table S2. LC/MS/MS protein composition data from a 39-year-old male ILM. Sheet 1 summarizes the total proteome, and selected ECM proteins are listed in Sheet 2.

Table S3. LC/MS/MS protein composition data from a 54-year-old female ILM. Sheet 1 summarizes the total proteome, and selected ECM proteins are listed in Sheet 2.